Inorganic Chemistry

ARTICLE

pubs.acs.org/IC

Synthesis and Crystal Structure of a Layered Silicate HUS-1 with a Halved Sodalite-Cage Topology

Takuji Ikeda,*[,†] Yasunori Oumi,[‡] Koutaro Honda,[§] Tsuneji Sano,[§] Koichi Momma,[∥] and Fujio Izumi[∥]

[†]Research Center for Compact Chemical Systems, National Institute of Advanced Industrial Science and Technology, AIST Tohoku, Sendai, Miyagi 983-8551, Japan

[‡]Life Science Research Center, Gifu University, Gifu 501-1193, Japan

[§]Department of Applied Chemistry, Graduate School of Engineering, Hiroshima University, Higashi-Hiroshima 739-8527, Japan

[∥]Quantum Beam Center, National Institute for Materials Science, 1-1 Namiki, Tsukuba, Ibaraki 305-0044, Japan

Supporting Information

ABSTRACT: A new layered silicate, HUS-1, was synthesized by hydrothermal synthesis using decomposed **FAU**- and ***BEA**-type zeolites as nanosized silica parts. Structural analyses by X-ray powder diffractometry and solid-state magic-angle-spinning (MAS) NMR spectroscopy revealed that HUS-1 has a layered structure containing a silicate layer per unit cell along a stacking direction. Its framework topology is similar to that of **SOD**-type zeolites and consists of a halved sodalite cage, which includes four- and six-membered Si rings. Structure refinement by the Rietveld method showed that tetramethylammonium (TMA) ions used as a structure-directing agent (SDA) were incorporated into the interlayer. The four methyl groups of the TMA molecule were located orderly in a hemispherical cage in the silicate layer, which suggests restraint of molecular motion. The interlayer distance is estimated at about 0.15 nm, which is unusually short in comparison with that in other layered silicates (e.g., β-HLS or RUB-15) with similar framework topologies. The presence of hydrogen bonding between adjacent terminal O atoms was clearly revealed by the ^{1}H MAS NMR spectroscopy and by electron-density distribution obtained by the maximum entropy method.

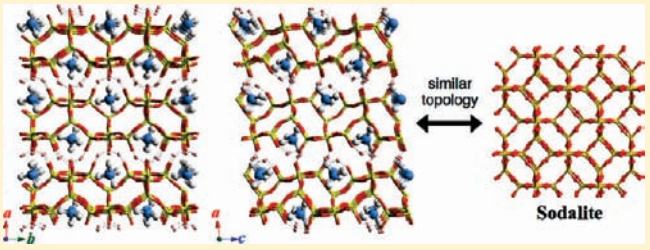

1. INTRODUCTION

Layered silicates are among important industrial materials, and their use as a flexible silica material has attracted the interest of many researchers. So far, layered silicates have been used as a silica source for the synthesis of various mesoporous materials or other silicates. For example, mesoporous FSM-16 and KSW-2 were synthesized from clay-like layered silicate kanemite and magadiite, respectively,[1,2] and a zeolite offretite and a layered silicate FLS-1 were synthesized from magadiite.[3,4] Moreover, layered silicates have been adopted for new zeolite syntheses, as nanosized blocks in the topotactic conversion method. For example, **CDO** (the three characters indicate the framework-type code),[5] **NSI**,[6] **CAS-NSI**,[7] **RWR**,[8−10] and **RRO**[11]-type zeolites have been prepared using layered silicates PLS-1[5] (isomorphic materials: PLS-4,[12] RUB-36,[13,14] MCM-47,[15] MCM-65,[16] UZM-13,[17] UZM-17,[17] UZM-19[17]), Nu-6(1),[6] EU-19,[7,18] RUB-18,[19] and RUB-39,[20] respectively. In this method, frameworks of layered silicates are used like a Lego block, without destruction of their framework structures.

It is also known that layered silicates β-HLS[21] and RUB-15[22] (isomorphic material: DLM-2[23]) have a zeolitic framework composed of a halved sodalite cage. In both compounds, tetramethylammonium (TMA) cations are located in the interlayer. Sodalite (**SOD**-type zeolite),[24] one of the most traditional zeolites, is constructed by connecting sodalite cages. The sodalite cage is a truncated octahedral cage composed of four- and six-membered Si rings; the effective window diameter is therefore small, about 0.22 nm, at the six-membered ring.

The framework structures of both β-HLS and RUB-15 are in part identical to that of sodalite, and the structural difference between them is the cutting direction in the sodalite structure (Figure 1). The β-HLS framework can be formed by clipping the sodalite cage along the [100] direction, whereas the framework of RUB-15 is formed by clipping along the [110] direction. Li and co-workers[25] reported a new layered silicate RUB-51 which includes the bulky benzyltrimethylammonium hydroxide in the interlayer. The RUB-51 framework structure is the same as that of RUB-15. Moteki et al.[26] reported that high-silica sodalite, whose pore openings are not occluded, can be obtained from RUB-15 by topotactic conversion via lamellar intermediates prepared by treatment with acetic acid. They also first demonstrated that the resultant high-silica sodalite has high hydrogen-adsorption capabilities.

In this work, we found a new type of a layered silicate, HUS-1 (Hiroshima University Silicate-1), with a halved **SOD**-type framework structure; the silicate was obtained based on the interzeolite conversion method. Recently, Sano and co-workers

Received: October 1, 2010
Published: February 04, 2011

dx.doi.org/10.1021/ic1020065 | *Inorg. Chem.* 2011, 50, 2294–2301

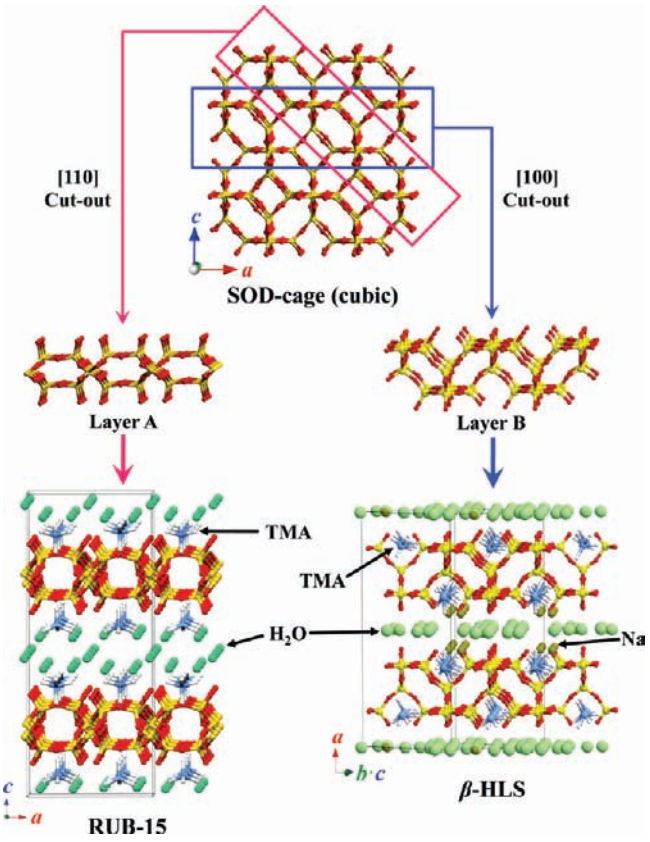

Figure 1. Structural relationship between the layered silicates, RUB-15 and β-HLS. Both framework topologies are similar to that of **SOD**-type zeolite.

have demonstrated that various zeolites can be prepared by this method using a decomposed zeolite **FAU** as nanosized silica parts. The key concept of the interzeolite conversion method, which is a bottom-up building process, has been described elsewhere.[27] To date, **CHA**, ***BEA**, **RUT**, **LEV**, **MTN**, and **OFF**-type aluminosilicate zeolites have been synthesized by this method with tetraalkylammonium cations as a SDA molecules.[28−33] The layered silicate HUS-1 was synthesized hydrothermally using two kinds of zeolites, that is, **FAU** and ***BEA**. The crystal structure and physicochemical properties of HUS-1 were investigated in detail by X-ray powder diffractometry (XRPD), solid-state magic-angle-spinning nuclear magnetic resonance (MAS NMR) spectroscopy, and thermogravimetric-differential thermal analysis (TG-DTA).

2. EXPERIMENTAL SECTION

2.1. Synthesis of HUS-1. The starting **FAU** and ***BEA** zeolites were prepared from NH_4−Y zeolite (Si/Al = 2.8, Tosoh Co., Japan) and H-*BEA (Si/Al = 21, Tosoh Co., Japan) by dealumination with H_2SO_4 (0.44 M) at 75 °C for 4 h. The interzeolite conversion was performed as follows. Two types of primary gels including silica nanosized parts were prepared. One was prepared by decomposition of dealuminated **FAU** zeolite by hydrothermal treatment with tetramethylammonium hydroxide (TMAOH, 20 wt %, Aldrich, U.S.A.) at 398 K for 24 h. The gel composition was Si/Al = 22, H_2O/SiO_2 = 5.5, and TMAOH/SiO_2 = 0.2. The other primary gel was prepared by decomposition of dealuminated ***BEA** zeolite by hydrothermal treatment with benzyltrimethylammonium hydroxide (BTMAOH, 40 wt %, Aldrich, U.S.A.) at 398 K for 24 h. The gel composition was Si/Al = 78, H_2O/SiO_2 = 5.5, and BTMAOH/SiO_2 = 0.8.

The resultant primary gels were mixed well with an aqueous solution of NaOH, and then the mixture was placed in a Teflon-lined stainless steel autoclave with a volume of 30 cm^3. The composition of the gel mixture was Si/Al = 50, TMAOH/SiO_2 = 0.1, BTMAOH/SiO_2 = 0.4, NaOH/SiO_2 = 0.2, and H_2O/SiO_2 = 5.5. The hydrothermal conversion was conducted at 398 K for 7−21 d in a convection oven. The solid product was collected by centrifugation and washed thoroughly with deionized water until filtrates became nearly neutral and then dried overnight at 70 °C.

2.2. Physicochemical Analyses. For accurate structural analyses, XRPD data were collected at room temperature on an ADVANCE D8-Vαrio1 (Bruker AXS, Japan) powder diffractometer with a modified Debye−Scherrer geometry and Cu $K\alpha_1$ radiation from a Ge(111) primary monochromator. The diffractometer was equipped with a linear position-sensitive detector VÅNTEC-1 (2θ coverage of 8°) and operated at 40 kV and 50 mA. The samples were sealed in borosilicate capillary tubes with an inner diameter of 0.7 mm. The μr (μ: linear absorption coefficient, r: sample radius) values of these sample tubes, which were determined by transmittance measurements, were 0.33, which was used for X-ray absorption corrections.

Crystal morphology was observed using an S-4800 (Hitachi, Japan) field emission scanning electron microscope (FE-SEM) operated at an acceleration voltage of 1 kV. Before the observation, all the samples were coated with an ion liquid (IL) of 1-butyl-3-methylimidazolium tetrafluoroborate (BMI-BF, Tokyo Chemical Industry Co., Inc.). The dilution of IL to a concentration of about 10% by methanol was effective for coating thin layers of IL on the sample. Coating of insulating samples (such as anhydrous silicate) with IL is effective in providing electronic conductivity to the samples, like metal coating by vacuum vapor deposition, that is, the electrification of the samples can be reduced remarkably.[34] Thermogravimetric analysis was carried out on a TG-DTA 2100 (MAC Science, Co. Ltd., Japan) in dry air at a heating rate of 10 K/min. The amount of intercalated molecules was estimated from the resulting TG-DTA curves. The chemical composition was roughly estimated by energy-dispersive X-ray (EDX) spectroscopy with EMAX EX-350 (HORIBA, Japan) attached to the above FE-SEM. Especially, carbon, hydrogen, and nitrogen contents of HUS-1 were determined by using a Yanaco CHN corder MT-6 in detail.

Solid-state ^1H-^{29}Si dipolar-decoupled (DD) MAS NMR spectra were measured with a spinning frequency of 5 kHz using a 4 mm MAS probe, a 90° pulse length of 3.6 μs, and a cycle delay time of 100 s on an AVANCE 400 WB spectrometer (Bruker BioSpin, Japan) operated at 79.495 MHz. Solid-state ^1H-^{29}Si cross-polarization (CP) MAS NMR spectra were also measured, with a contact time of 4 ms. The ^{29}Si chemical shift was calibrated with a standard sample of tetramethylsilane (TMS). The ^1H and ^{27}Al MAS NMR spectra were measured with a spinning frequency of 12 kHz and a single pulse sequence operated at 104.26 MHz for ^{27}Al and 400.13 MHz for ^1H. Furthermore, the ^1H-^{13}C CP MAS NMR spectra were also measured with a spinning frequency of 5 kHz, a 90° pulse length of 4.7 μs, and a cycle delay time of 5 s (operated at 100.613 MHz). The ^1H, ^{13}C, and ^{27}Al chemical shifts were referenced to TMS, glycine, and an aqueous solution of $AlCl_3$ (1 mol/dm^3), respectively.

2.3. Structural Analysis. The crystal structure of HUS-1 was determined by ab initio structural analysis. Indexing of reflections with the programs DICVOL91[35] and *N*-TREOR built in the program EXPO2009[36] successfully gave lattice parameters and indices of the reflections. The space group was determined from reflection conditions derived from these indices. Observed integrated intensities, $|F_{obs}|^2$, were extracted by the Le Bail method[37] using EXPO2009. Then, a structural model for HUS-1 was constructed by combination of the powder charge-flipping (pCF) method using Superflip[38,39] and the direct method with EXPO2009.

dx.doi.org/10.1021/ic1020065 |*Inorg. Chem.* 2011, 50, 2294–2301

Table 1. Conditions of the XRPD Experiment and Parts of Data Related to the Rietveld Refinement for Layered Silicate HUS-1

compound name	HUS-1
estimated chemical formula	$Si_{10}O_{24}H_6 \cdot 2[(CH_3)_4N]$
F_W	819.18
space group	$P2_1$ (No. 4)
a/Å	8.95561(19)
b/Å	9.21294(13)
c/Å	8.74207(12)
β/deg	95.831(2)
unit-cell volume, V/Å^3	717.55(13)
wavelength, λ/Å	1.540593 (Cu Kα_1)
2θ range/deg	8.0−100.1
step size, 2θ/deg	0.017368
counting time per step/s	32624
profile range in the unit of fwhm	14
fwhm/deg (at 2θ = 16.566°)	0.246
no. of intensity data	5304
no. of contributing reflections	799
no. of refined structural parameters	115
no. of background parameters	12
no. of nonlinear restraints	102
R_F (Rietveld)	0.0080
R_B (Rietveld)	0.0079
R_{wp} (Rietveld)	0.0231
R_e (Rietveld)	0.0145
R_F (MEM_final)	0.0076
R_{wp} (MEM_final)	0.0051

Lattice and structure parameters of HUS-1 were refined by the Rietveld method using the program RIETAN-FP[40] on the basis of the above structural model. A split pseudo-Voigt profile function and a background function of Legendre polynomials with 11th order were used in the refinement. Partial profile relaxation[41] with a modified split pseudo-Voigt function was applied to some reflections with highly asymmetric profiles. In the early stage of the refinement, we imposed restraints upon all the Si−O bond lengths, that is, l(Si−O) = 1.60 ± 0.02 Å, all the O−Si−O bond angles, that is, ϕ(O−Si−O) = 109.47 ± 2.0°. Furthermore, restraints were imposed upon all the N−C bond lengths, that is, l(N−C) = 1.49 ± 0.03 Å, all the C−H bond lengths, that is, l(C−H) = 1.08 ± 0.02 Å, all the C−N−C, N−C−H, and H−C−H bond angles, that is, ϕ(C−N−C) = ϕ(N−C−H) = ϕ(H−C−H) = 109.47 ± 3.0°, which are based on the molecular geometry of TMA, in the final stage of the structure refinement. Degrees of restraints were gradually decreased with progress in the structure refinement.

Electron-density distribution (EDD) in the unit cell of HUS-1 was calculated from the observed structure factors, F_{obs}, by the maximum entropy method (MEM) using the program Dysnomia.[42] After the first MEM analysis, EDD was redetermined by MEM-based pattern fitting (MPF).[40] The MPF analysis, which is an alternate repetition of whole-pattern fitting and MEM analyses, is very effective in visualizing chemical bonds and disordered arrangements of chemical species such as interlayer organic molecules. Table 1 summarizes experimental conditions of the XRPD measurement and parts of the results of the Rietveld refinement for HUS-1. The final structural model and electron density distribution were visualized using the program VESTA.[43]

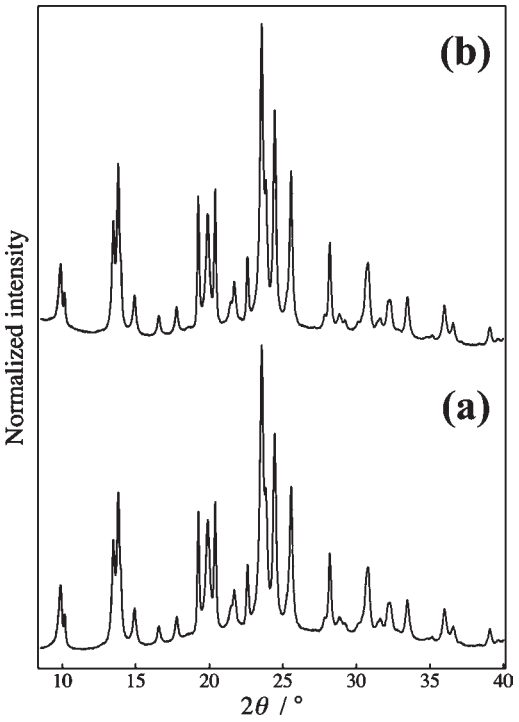

Figure 2. XRPD patterns of HUS-1 synthesized with reaction times of (a) 7 d and (b) 21 d using CuKα_1 radiation.

3. RESULTS AND DISCUSSION

3.1. PXRD, SEM, and TG-DTA Analysis. Figure 2 shows XRPD patterns of the samples of HUS-1. Crystal growth of HUS-1 was finished almost completely after a reaction time of 7 d. Although the crystallinity of the resultant HUS-1 after reaction for 7 d was moderate, it was somewhat improved by extending the reaction time to 21 d. We will hereinafter describe only the product resulting from the reaction for 21 d.

A SEM image in Figure 3 shows that the product shape has the form of square plates with a size up to an area of 2 μm × 4 μm and a thickness up to 0.8 μm. The plate crystals were found to be stacks of thin layers, and their surfaces were rough with large voids. These findings suggest that HUS-1 has a typical layered structure. From EDX analysis, Al and Na were hardly detected in the product. Carbon, hydrogen, and nitrogen contents of HUS-1 were estimated at 11.28 wt %, 3.37 wt %, and 3.37 wt %, respectively, indicating total amount of organic content of 18.02 wt %. This means that atomic ratio of the organic species in the product is C/H/N = 3.9:13.8:1.0.

A large weight loss of about 23 wt %, which is larger than that of organic content estimated by CHN analysis, was observed in TG-DTA curves in a temperature range 573−630 K (Figure 4). A strong exothermic peak was also observed at 623 K. This result suggests that observed large weight loss is derived from combustion of intercalated organic species and dehydration condensation of layered framework (see section 3.3). The weight loss at temperatures lower than 473 K was only about 1 wt %, which provides evidence for a small amount of adsorbed water molecules in the interlayers; that is, HUS-1 is regarded as an anhydrous layered silicate. Additionally, the gradual weight loss of about 3 wt % was observed at >630 K, which is due to dehydration condensation of silanols in the framework.

dx.doi.org/10.1021/ic1020065 |*Inorg. Chem.* 2011, 50, 2294–2301

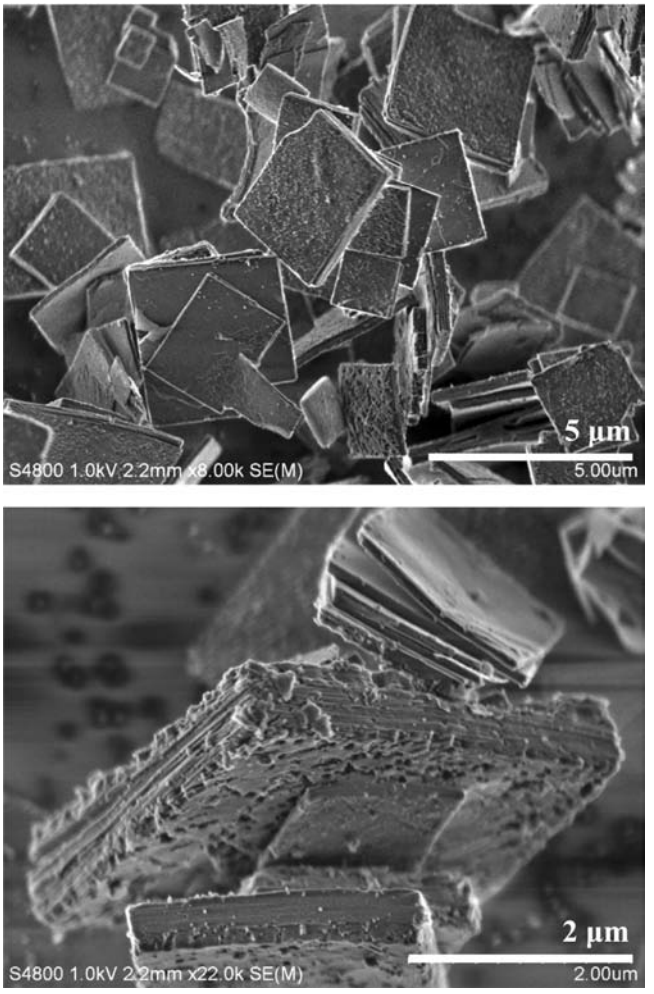

Figure 3. SEM micrographs of HUS-1. The upper and lower images show square-shaped plate morphology and the rough surfaces, respectively.

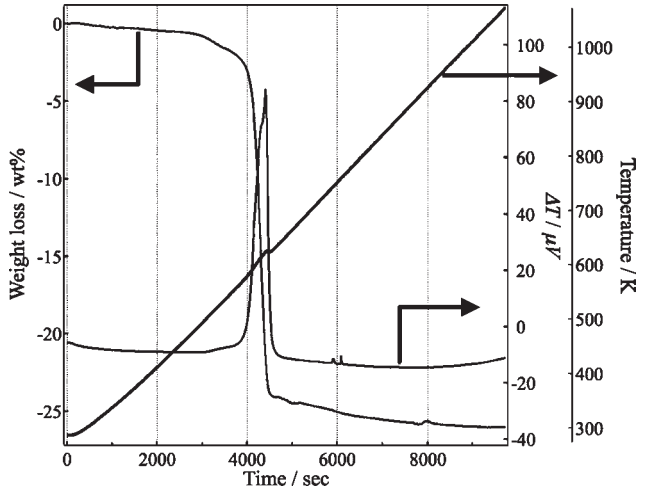

Figure 4. TG, DTA, and temperature curves in the thermal analysis of HUS-1.

3.2. Solid-State NMR. First, NMR spectroscopy probes all samples in the specimen container including the amorphous part. Accordingly, the signal of the amorphous fraction overlaps the signal of the crystalline sample more or less. Figure 5 gives a ^{1}H-^{13}C CP MAS NMR spectrum of HUS-1. A sharp resonance peak observed at 57.4 ppm is attributed to a methyl group, which presents evidence that only TMA cations are intercalated. This result, that is, the presence of TMA molecule with a molecular formula of $C_4H_{12}N$, was well consistent with the atomic ratio of C:H:N = 3.9:13.8:1.0 determined by the CHN analysis. BTMA cations are believed to be either absent in HUS-1 or decomposed into TMA cations during the hydrothermal conversion. BTMA is, in general, not converted into TMA. However, a puzzling phenomenon was observed in the synthesis of zeolite **MTN** by interzeolite conversion.[32] Moreover, a ^{13}C NMR spectrum of the primary gel including zeolite ***BEA** and BTMA cations showed the inclusion of BTMA cations.

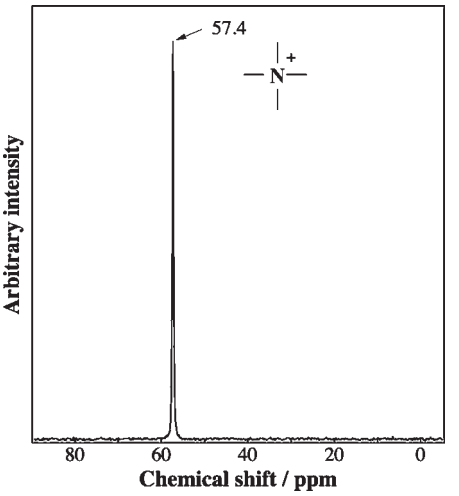

Figure 5. ^{1}H-^{13}C CP MAS NMR spectrum of HUS-1.

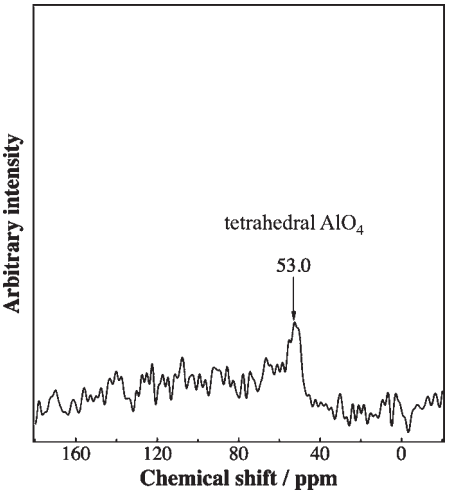

Figure 6. ^{27}Al MAS NMR spectrum of HUS-1.

The presence of a tetrahedral Al site was detected in a ^{27}Al MAS NMR spectrum (Figure 6). However, the intensity of the peak was very small with a low S/N ratio despite accumulation of 5120 scans for this spectrum. The amount of Al atoms in the HUS-1 framework is, therefore, negligible. Further, a peak due to an octahedral Al site was hardly detected near 0 ppm. These findings are nearly consistent with the result of EDX analysis. Thus, in our structure refinement, we regarded that HUS-1 contains no Al atoms.

dx.doi.org/10.1021/ic1020065 |*Inorg. Chem.* 2011, 50, 2294–2301

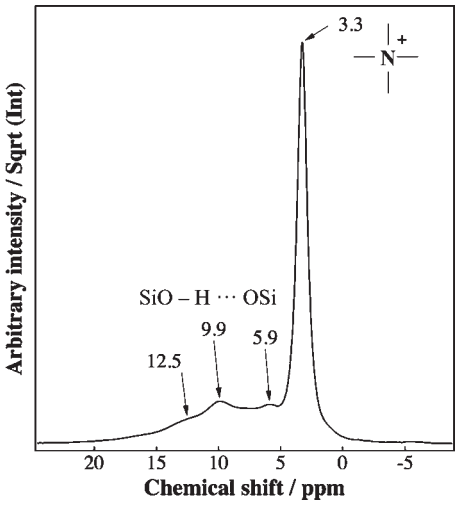

Figure 7. ^{1}H MAS NMR spectrum of HUS-1; the *y* axis is displayed in a square-root scale.

Figure 7 shows a ^{1}H MAS NMR spectrum of HUS-1. A resonance peak attributed to a methyl group was observed at 3.3 ppm. Three broad resonance peaks at 5.9 ppm, 9.9 ppm, and 12.5 ppm are due to the SiO−H···OSi hydrogen bonding of silanol groups. The atomic distances, d(O−O), between adjacent silanols were estimated at 2.78 Å, 2.64 Å, and 2.56 Å from the downfield shift, which is described as δ/ppm = 90.3 − 30.4 × d(O−H···O)/Å.[44] This finding suggests that the hydrogen bonding is formed in the interlayer or intralayer.

An ^{29}Si MAS NMR spectrum showed inclusion of a large amount of Q^3 [(−SiO)$_3$Si−OH] structures in the HUS-1 framework. Three Q^3 resonance peaks were observed at −102.7 ppm, −105.6 ppm, and −107.5 ppm although a single Q^4 [(−SiO)$_4$Si] resonance peak was observed at −114.6 ppm in a ^{1}H-^{29}Si DD MAS NMR spectrum (Figure 8a). The peak intensity ratio of Q^3/Q^4 was estimated at about 4.4 by curve fitting with a Lorentz function. The ^{1}H-^{29}Si CP MAS NMR spectrum of HUS-1 was similar to the DD MAS NMR spectrum (Figure 8b) though intensities of Q^3-peaks increased with sharper peak widths. These findings support the idea that HUS-1 has a layered structure with a large number of silanols on the layer surface.

3.3. Structural Analysis. The indexing of the reflections gave a monoclinic unit cell of a = 0.8973 nm, b = 0.9214 nm, and c = 0.8748 nm, β = 95.83° with acceptable figures of merit: $F17$ = 32 and $M17$ = 55. Reflection conditions derived from the indexed reflections were $k = 2n$ for $0k0$, which gives two possible space groups: $P2_1$ and $P2_1/m$. Assuming that HUS-1 is centrosymmetric, we tentatively adopted $P2_1/m$ (No. 11, setting 1).

$|F_{obs}|^2$ values of 798 reflections in the region d > 0.1 nm were extracted by the Le Bail method. We, at first, attempted to solve the framework structure of HUS-1 by the direct method, but no solution was obtained. Next, we applied the *p*CF method to obtain the framework structure and detected four Si and five O sites. The framework topology composed of four- and six-membered rings were clarified at this stage. Observed values of $|F_{obs}|^2$ were then re-extracted by the Le Bail method using RIETAN-FP on the basis of the partial structural information and analyzed by the direct-method with EXPO2009. Consequently, three additional O sites attributed to terminal silanols were successfully located. As figure 9 illustrates, its topology is

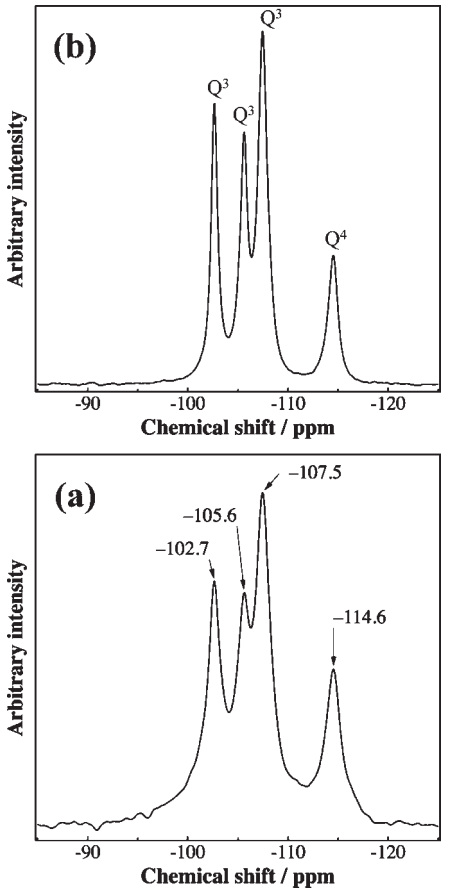

Figure 8. (a) ^{1}H-^{29}Si DD MAS NMR and (b) ^{1}H-^{29}Si CP MAS NMR spectra of HUS-1.

identical to that of a halved **SOD**-type framework. A few atoms attributed to a TMA cation were further found in a hemispherical space. Additional analytical procedures are described in Supporting Information (Figure S1 and S2).

All the sites, that is, four Si and eight O sites in the asymmetric unit, derived in the above way were included as the initial structural model of the Rietveld refinement. The fractional coordinates of a virtual atom corresponding to a TMA cation, which has a scattering amplitude equivalent to $(CH_3)_4N$, in a hemispherical space were also refined because the atomic configuration of the TMA cation could not be determined unambiguously. This finding, coupled with the results of the TG-TDA and ^{13}C MAS NMR measurements, shows the presence of TMA molecules in the interlayer. At this stage, the reliability indices, R_{wp} and R_B, reached 3.5% (S = 2.4) and 2.0%, respectively.

The distribution of TMA cations in the hemispherical cage was investigated by the direct-space method with the program FOX.[45] In this analysis, the molecular structure of the TMA cation plus an H atom were introduced into a structural model as a single atomic group with bond lengths and angles restrained within very narrow regions. In addition, the positions of all the framework atoms were fixed at the positions determined by the Rietveld analysis. As a result, two equivalent TMA molecules overlapped along the b axis appeared in the hemispherical cage, and the positions of the H atoms of the molecule were too close to the framework atoms, which suggests that the space-group symmetry, $P2_1/m$, assumed thus far is quite inadequate. We, therefore, reconstructed the previous model according to the

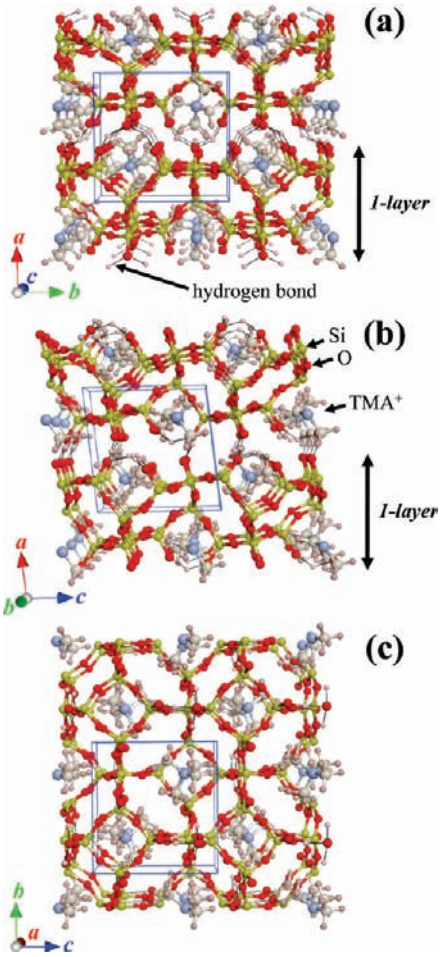

Figure 9. Structural model of HUS-1 viewed along the (a) [001], (b) [010], and (c) [100] directions.

space-group symmetry of $P2_1$ (No. 4), which is a maximal non-isomorphic subgroup of $P21/m$.[46] The transformation from the centrosymmetric space group $P2_1/m$ to the noncentrosymmetric $P2_1$ enables a pair of positions, (x, y, z) and $(-x, -y, -z)$, to become independent. Among the four known Si atoms, three of them, which are in special positions in the space group $P2_1/m$, are still kept, and one Si atom is split into two sites. Among the oxygen atoms, four sites in the $P2_1/m$ model were split, resulting in eight sites, and the other oxygen sites are not doubled. The TMA molecule was located near the center of the hemispherical cage with its molecular orientation determined clearly. Each atomic position of TMA obtained in this way was used for the model reconstruction.

The EDD obtained by MPF strongly suggests the presence of hydrogen bonds between terminal oxygen sites O1−O3, O1−O4, and O1−O7. Three proton sites at (0.47, 0.88, 0.17) for site H18, (0.49, 0.61, 0.20) for site H19, and (0.55, 0.25, 0.67) for site H20 were then added to the structural model because these positions corresponded to weighted centers of the hydrogen bonds in the EDD images. The scattering amplitude of H was added to site O7 in a terminal silanol group to maintain the charge balance.

In the final Rietveld refinement, 5 Si, 12 O, 1 N, 4 C, and 15 H sites were included in the asymmetric unit. All the isotropic atomic displacement parameters, B, for the Si sites were constrained to be

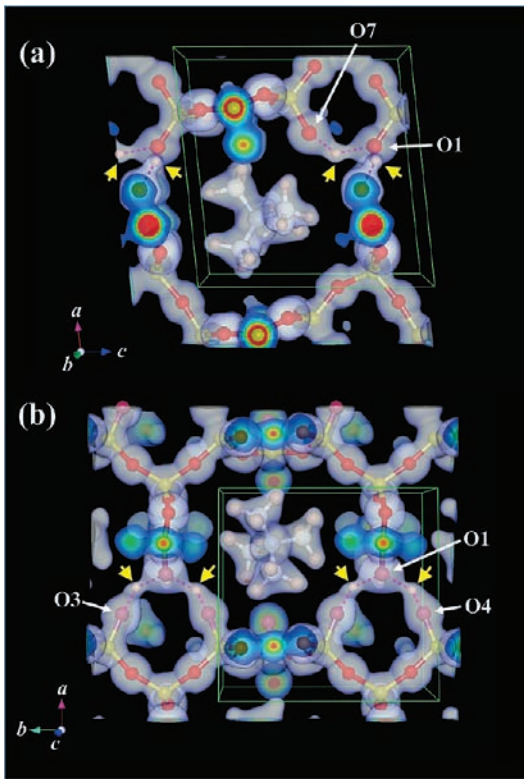

Figure 10. EDD images of HUS-1 obtained by the MPF analysis: (a) electron densities ($0 < y < 0.51$) viewed along the b axis, and (b) electron densities ($0.43 < z < 1.0$) viewed along the c axis. The spatial resolution was 90 × 92 × 88 pixels per unit cell.

equal: B(Si1) = B(Sin: n = 2−4). Simple approximations of B(O1) = B(On: n = 2−12) and B(Cn: n = 1−4) = B(N5) = B(Hn: n = 6−17) were also imposed on the B parameters of the O sites and of the C, N, and H sites, respectively. The B values of the H18, H19, and H20 sites were fixed at 5.0 Å^2 for convenience. Finally, R factors were decreased to sufficiently low levels, that is, R_{wp} = 2.3% (S = 1.6) and R_B = 0.8% (Table 1).

The chemical formula of HUS-1 was estimated to be $Si_{10}O_{24}H_6 \cdot 2[(CH_3)_4N]$ according to the results of the structure refinement. The resulting organic content, which was calculated to be 18.05 wt %, agreed with those determined by the CHN analysis (ca. 18.0 wt %) very well. If we suppose that HUS-1 changes to amorphous silica completely (i.e., $Si_{10}O_{24}H_6 \cdot 2[(CH_3)_4N] \rightarrow Si_{10}O_{20}$), the total weight loss is calculated as 26.7 wt %, which is almost in agreement with the observed weight loss of 26.0 wt % by the TG-DTA analysis. Although a small amount of silanols might remain because of incomplete condensation, the TG result strongly supports the chemical formula estimated by the structure analysis. Thus, it was found that the result of the chemical analysis coincides with the structure model of HUS-1.

Figure 9 shows the structural model of HUS-1 obtained finally. The narrowest width between adjacent layers was estimated at about 0.15 nm (Figure 11 and Supporting Information, Figure S4). The lattice parameter, a, approximately corresponds to the thickness of the silicate layer. The projection of the silicate layer along the [100] direction coincides with that of the sodalite structure along the [100] direction (Figure 9c). The nearest atomic distances between neighboring silanol groups, l(O−O),

dx.doi.org/10.1021/ic1020065 |Inorg. Chem. 2011, 50, 2294–2301

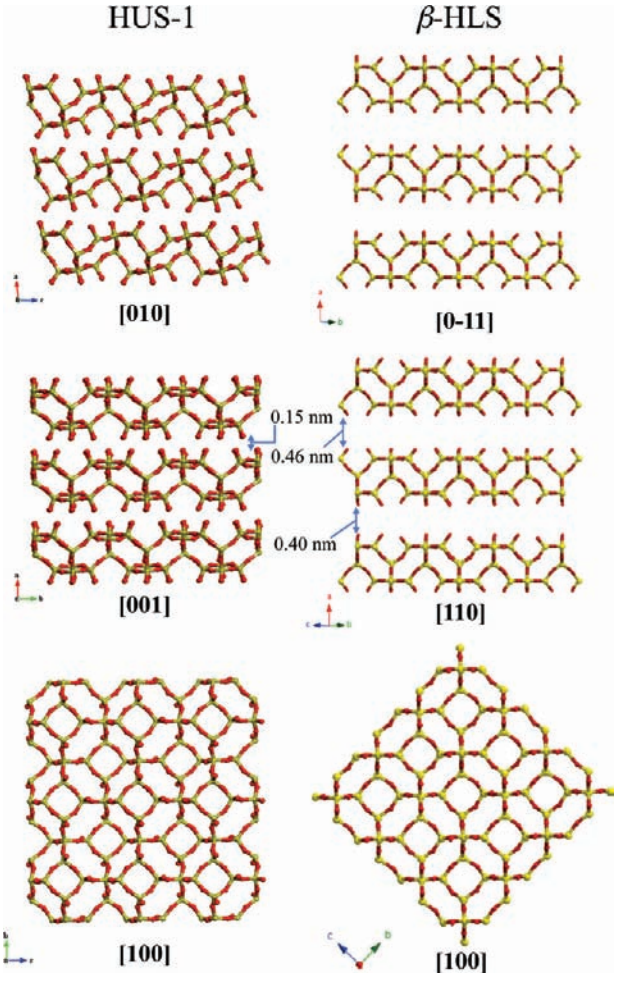

Figure 11. Schematic representations of the framework structures for HUS-1 and *β*-HLS. The upper and middle figures show stacking sequences of silicate layers in HUS-1 and *β*-HLS, respectively, while the lower figure illustrates the identical framework topology of both layers.

were *l*(O1−O3) = 2.64(3) Å, *l*(O1−O4) = 2.53(6) Å, and *l*(O1−O7) = 2.69(2) Å, which are in good agreement with the values, that is, 2.56 Å, 2.64 Å, and 2.78 Å, estimated from the ^{1}H MAS NMR spectrum. Additionally, calculated Q^3/Q^4 ratio on the basis of the framework geometry is 4.0, which was smaller than the value (ca. 4.4) estimated by the ^{29}Si DDMAS NMR spectrum. This fact suggests that there is a small amount of Si atom defects in framework. The position of the defective site, however, could not be determined unambiguously by the structure refinement because of moderate crystallinity of the sample. Tables S1 and S2 (see Supporting Information) list structure and geometrical parameters obtained by the Rietveld analysis of HUS-1, respectively. Supporting Information, Figure S3 shows observed, calculated, and difference patterns. The average bond length *l*(Si−O) and bond angle *ϕ*(O−Si−O), which are close to expected values, fall within 1.55−1.64 Å and 106.1−114.1°, respectively.

Figure 10 shows EDD images of HUS-1 obtained by the MPF analysis. Electron densities attributed to hydrogen bonding were clearly seen between sites O1 and O7 (Figure 10a). Similarly, electron densities are observed between sites O1 and O3 and between sites O1 and O4 (Figure 10b). These findings support the idea that adjacent layers are bridged by hydrogen bonding to form a pseudo-spherical cage, with an internal diameter of about 0.65 nm, in the interlayer. Because the EDD determined by MPF shows the ordered arrangement of TMA in the pseudo-cage, the TMA molecules are believed to be cations. Furthermore, molecular motion of TMA is estimated to be considerably restricted. The MPF analysis lowered R_{wp}(MEM) from 0.75% to 0.51% and R_F(MEM) from 0.82% to 0.77% after four cycles.

4. STRUCTURAL COMPARISON OF HUS-1 AND *β*-HLS

Figure 11 illustrates the framework structures of HUS-1 and *β*-HLS[20] viewed along three different directions. The stacking sequence of neighboring layers in HUS-1 is completely different from that in *β*-HLS. The layers in HUS-1 are alternately stacked with shifts of 0.5*b* and 0.5*c* along the [010] and [001] directions, respectively, compared with those in *β*-HLS. In fact, the crystal structure of HUS-1 is formed in an *AAAA* stacking order whereas that of *β*-HLS is formed in an *ABAB* stacking order. Their framework topologies are similar to each other. However, the framework of HUS-1 is somewhat asymmetric in comparison with the symmetric framework geometry of *β*-HLS or sodalite.

The interlayer distance in *β*-HLS is much larger than that in HUS-1. Adsorbed water molecules and Na^+ ions are densely distributed in the *β*-HLS[20] interlayer (Figure 1), but a small amount of H^+ ions contributing to hydrogen bonding is distributed in the HUS-1 interlayer. In both compounds, TMA cations are known to be accommodated in halved sodalite cages. From the structural model obtained in the present study, we can safely guess that HUS-1 is not transformed into sodalite by direct calcination. Although, HUS-1 was changed to an amorphous phase by calcination, a structural transformation may be achieved by some chemical modifications. For example, like IEZ[47−49] or APZ[50] series, which are prepared from various layered silicates, interlayer expansion may be possible even in HUS-1 by silylation or acid treatment because no extra-framework atoms exist in the interlayer except for TMA cations in the hemispherical cage.

5. CONCLUSIONS

We synthesized a new layered silicate HUS-1, whose chemical composition is $Si_{10}O_{24}H_6 \cdot 2(TMA)$, based on the interzeolite conversion method. Silica and alumina sources were prepared by decomposition of **FAU** and ***BEA** zeolites under hydrothermal conditions, but Al atoms were hardly included in the HUS-1 framework. The crystal structure of HUS-1, with a halved **SOD**-type framework topology, is very similar to that of *β*-HLS though the topology was deformed in comparison with that of *β*-HLS. The TMA molecule in the hemispherical sodalite cage acted as an SDA. The interlayer distances between neighboring silicate layers are very short because neighboring layers are bridged by hydrogen bonding between terminal silanols. The presence of hydrogen bonding was clearly revealed by ^{1}H MAS NMR spectra and EDD images resulting from MPF analysis. The hydrogen bonds stabilize the whole crystal structure to form small pseudo-cages like sodalite cage.

■ ASSOCIATED CONTENT

Supporting Information. Figure showing of crystal structure models for HUS-1 by using the *p*CF and the direct method analyses and observed, calculated, and difference patterns obtained

dx.doi.org/10.1021/ic1020065 |*Inorg. Chem.* 2011, 50, 2294–2301

by the Rietveld refinement for HUS-1 and framework topology of HUS-1, and tables of structural parameters and bond lengths and bond angles of HUS-1. This material is available free of charge via the Internet at http://pubs.acs.org.

AUTHOR INFORMATION

Corresponding Author
*E-mail: takuji-ikeda@aist.go.jp. Phone: +81-22-237-3016.

ACKNOWLEDGMENT

This work was partly supported by Grand-in-Aid [No. 20310066] from JSPS, Japan.

REFERENCES

(1) Kimura, T.; Kamata, T.; Fuziwara, M.; Takano, Y.; Kaneda, M.; Sakamoto, Y.; Terasaki, O.; Sugahara, Y.; Kuroda, K. *Angew. Chem., Int. Ed.* **2000**, *39*, 3855.
(2) Inagaki, S.; Fukushima, Y.; Kuroda, K. *J. Chem. Soc., Chem. Commun.* **1993**, 680.
(3) Wang, Y.; Shang, Y.; Wu, J.; Zhu, J.; Yang, Y.; Meng, C. *J. Chem. Technol. Biotechnol.* **2010**, *85*, 279.
(4) Kooli, F.; Kiyozumi, Y.; Rives, V.; Mizukami, F. *Langmuir* **2002**, *18*, 4103.
(5) Ikeda, T.; Akiyama, Y.; Oumi, Y.; Kawai, A.; Mizukami, F. *Angew. Chem., Int. Ed.* **2004**, *43*, 4892.
(6) Zanardi, S.; Alberti, A.; Cruciani, G.; Corma, A.; Fornes, V.; Brunelli, M. *Angew. Chem., Int. Ed.* **2004**, *43*, 4933.
(7) Marler, B.; Camblor, M. A.; Gies, H. *Microporous Mesoporous Mater.* **2006**, *90*, 87.
(8) Marler, B.; Ströter, N.; Gies, H. *Microporous Mesoporous Mater.* **2005**, *83*, 201.
(9) Oumi, Y.; Takeoka, T.; Ikeda, T.; Yokoyama, T.; Sano, T. *New J. Chem.* **2007**, *31*, 593.
(10) Ikeda, T.; Oumi, Y.; Takeoka, T.; Yokoyama, T.; Sano, T.; Hanaoka, T. *Microporous Mesoporous Mater.* **2008**, *110*, 488.
(11) Wang, Y.; Marler, B.; Gies, H.; Müller, U. *Chem. Mater.* **2005**, *17*, 43.
(12) Ikeda, T.; Kayamori, S.; Mizukami, F. *J. Mater. Chem.* **2009**, *19*, 5518.
(13) Song, J.; Gies, H. *Stud. Surf. Sci. Catal.* **2004**, *154A*, 295.
(14) Marler, B.; Wang, Y.; Song, H.; Gies, H. Abstracts of Papers, 15th International Zeolite Conference, 2007; Beijing, China, August 12−17, 2007; p 599.
(15) Burton, A.; Accardi, R. J.; Lobo, R. F.; Falcioni, M.; Deem, M. W. *Chem. Mater.* **2000**, *12*, 2936.
(16) Dorset, D. L.; Kennedy, G. J. *J. Phys. Chem. B* **2004**, *108*, 15216.
(17) Knight, L. M.; Miller, M. A.; Koster, S. C.; Gatter, M. G.; Benin, A. I.; Willis, R. R.; Lewis., G. J.; Broach, R. W. *Stud. Surf. Sci. Catal.* **2007**, *170A*, 338.
(18) Blake, A. J.; Franklin, K. R.; Lowe, B. M. *J. Chem. Soc., Dalton Trans.* **1988**, 2513.
(19) Vortmann, S.; Rius, J.; Siegmann., S.; Gies, H. *J. Phys. Chem. B* **1997**, *101*, 1292.
(20) Wang, Y. X.; Gies, H.; Lin, J. H. *Chem. Mater.* **2007**, *19*, 4181.
(21) Ikeda, T.; Akiyama, Y.; Izumi, F.; Kiyozumi, Y.; Mizukami, F.; Kodaira, T. *Chem. Mater.* **2001**, *13*, 1286.
(22) Oberhagemann, U.; Bayat, P.; Marler, B.; Gies, H.; Rius, J. *Angew. Chem., Int. Ed. Engl.* **1996**, *35*, 2869.
(23) Massüger, L.; Baerlocher, C.; McCusker, L. B.; Zwijnenburg, M. A. *Microporous Mesoporous Mater.* **2007**, *105*, 75.
(24) Pauling, L. *Z. Kristallogr.* **1930**, *74*, 213.
(25) Li, Z.; Marler, B.; Gies, H. *Chem. Mater.* **2008**, *20*, 1896.
(26) Moteki, T.; Chaikittisilp, W.; Shimojima, A.; Okubo, T. *J. Am. Chem. Soc.* **2008**, *130*, 15780.
(27) Jon, H.; Sasaki, H.; Inoue, T.; Itakura, M.; Takahashi, S.; Oumi, Y.; Sano, T. *Stud. Surf. Sci. Catal.* **2008**, *174*, 229.
(28) Itakura, M.; Inoue, T.; Takahashi, A.; Fujitani, T.; Oumi, Y.; Sano, T. *Chem. Lett.* **2008**, *37*, 908.
(29) Jon, H.; Ikawa, N.; Oumi, Y.; Sano, T. *Chem. Mater.* **2008**, *20*, 4135.
(30) Jon, H.; Takahashi, T.; Sasaki, H.; Oumi, Y.; Sano, T. *Microporous Mesoporous Mater.* **2008**, *113*, 56.
(31) Inoue, T.; Itakura, M.; Jon, H.; Oumi, Y.; Takahashi, A.; Fujitani, T.; Sano, T. *Microporous Mesoporous Mater.* **2008**, *122*, 149.
(32) Sasaki, H.; Jon, H.; Itakura, M.; Inoue, T.; Ikeda, T.; Oumi, Y.; Sano, T. *J. Porous Mater.* **2009**, *16*, 465.
(33) Itakura, M.; Oumi, Y.; Sadakane, M.; Sano, T. *Mater. Res. Bull.* **2010**, *45*, 646.
(34) Arimoto, S.; Sugimura, M.; Kageyamaa, H.; Torimoto, T.; Kuwabata, S. *Electrochim. Acta* **2008**, *53*, 6228.
(35) Boultif, A.; Louër, D. *J. Appl. Crystallogr.* **1991**, *24*, 987.
(36) Altomare, A.; Camalli, M.; Cuocci, C.; Giacovazzo, C.; Moliterni, A.; Rizzi, R. *J. Appl. Crystallogr.* **2009**, *42*, 1197.
(37) Le Bail, A.; Duroy, H.; Fourquet, J. L. *Mater. Res. Bull.* **1988**, *23*, 447.
(38) Oszlányi, G.; Süto, A. *Acta Crystallogr., Sect. A* **2004**, *60*, 134.
(39) Palatinus, L.; Chapuis, G. *J. Appl. Crystallogr.* **2007**, *40*, 786.
(40) Izumi, F.; Momma, K. *Solid State Phenom.* **2007**, *130*, 15.
(41) Ohta, T.; Izumi, F.; Oikawa, K.; Kamiyama, T. *Phys. B* **1997**, *234−236*, 1093.
(42) Izumi, F.; Momma, K. *J. Vac. Soc. Jpn.* **2010**, *53*, 706−712.
(43) Momma, K.; Izumi, F. *J. Appl. Crystallogr.* **2008**, *41*, 653.
(44) Xue, X.; Kanzaki, M. *J. Phys. Chem. B* **2007**, *111*, 13156.
(45) Favre-Nicolin, V.; Cerny, R. *J. Appl. Crystallogr.* **2002**, *35*, 734.
(46) *International Tables for Crystallography*, 5th ed.; Hahn, Th., Ed.; Springer: Dordrecht, The Netherlands, 2005; Vol. A, pp 35−38.
(47) Inagaki, S.; Yokoi, T.; Kubota, Y.; Tatsumi, T. *Chem. Commun.* **2007**, 5188.
(48) Wu, P.; Ruan, J.; Wang, L.; Wu, L.; Wang, Y.; Liu, Y.; Fan, W.; He, M.; Terasaki, O.; Tatsumi, T. *J. Am. Chem. Soc.* **2008**, *130*, 8178.
(49) Ruan, J.; Wu, P.; Slater, B.; Zhao, Z.; Wu, L.; Terasaki, O. *Chem. Mater.* **2009**, *21*, 2904.
(50) Ikeda, T.; Kayamori, S.; Oumi, Y.; Mizukami, F. *J. Phys. Chem. C* **2010**, *114*, 3466.